How to cite: *Angew. Chem. Int. Ed.* **2023,** *62,* e202302394
doi.org/10.1002/anie.202302394

Electrocatalysis Hot Paper

Nano-Impact Single-Entity Electrochemistry Enables Plasmon-Enhanced Electrocatalysis**

*Sagar Ganguli[+], Ziwen Zhao[+], Onur Parlak, Yocefu Hattori, Jacinto Sá, and Alina Sekretareva**

Abstract: Plasmon-enhanced electrocatalysis (PEEC), based on a combination of localized surface plasmon resonance excitation and an electrochemical bias applied to a plasmonic material, can result in improved electrical-to-chemical energy conversion compared to conventional electrocatalysis. Here, we demonstrate the advantages of nano-impact single-entity electrochemistry (SEE) for investigating the intrinsic activity of plasmonic catalysts at the single-particle level using glucose electrooxidation and oxygen reduction on gold nanoparticles as model reactions. We show that in conventional ensemble measurements, plasmonic effects have minimal impact on photocurrents. We suggest that this is due to the continuous equilibration of the Fermi level (E_F) of the deposited gold nanoparticles with the E_F of the working electrode, leading to fast neutralization of hot carriers by the measuring circuit. The photocurrents detected in the ensemble measurements are primarily caused by photo-induced heating of the supporting electrode material. In SEE, the E_F of suspended gold nanoparticles is unaffected by the working electrode potential. As a result, plasmonic effects are the dominant source of photocurrents under SEE experimental conditions.

Introduction

In recent years, there has been a lot of interest in incorporating plasmonic nanomaterials into electrocatalytic systems to improve their electrocatalytic performance by selective utilization of UV and visible-light irradiation through localized surface plasmon resonance (LSPR) effects. Combining LSPR excitation with an electrochemical bias applied to the plasmonic material, known as plasmon-enhanced electrochemistry or plasmon-enhanced electrocatalysis (PEEC), has the potential to result in more efficient conversion of electrical energy to chemical energy and vice versa compared to conventional electrocatalysis.[1,2] Following LSPR excitation, several processes can contribute to increased electrocatalytic rates. First, LSPR excitation strongly enhances the electric field on the surface of the electrocatalyst.[3] Plasmonic field-enhanced photocatalytic water splitting and methylene blue transformation on silver nanoparticles in contact with TiO_2 have been demonstrated.[4,5] Further non-radiative decay of LSPR through Landau damping leads to the generation of non-thermally distributed highly energetic electrons and holes, with energies well above and below the Fermi level, respectively, on the surface of a plasmonic nanoparticle.[6] Electron-electron scattering prompts thermalization of these energetic charge carriers, forming a "warm" Fermi-Dirac distribution.[7] Non-thermal and thermalized carriers have been shown to facilitate various electrocatalytic reactions such as glucose,[8,9] methanol,[10–12] and glycerol[13] oxidation, ammonia,[14] proton[12,15] and oxygen reduction.[16] Finally, the internal decay of hot carriers inside a plasmonic nanoparticle can significantly heat the nanostructure and surrounding environment. Elevated temperatures near the plasmonic electrocatalyst facilitate phonon-driven chemical reactions.[17,18]

In electrocatalytic systems, plasmonic nanomaterials can act as both light-adsorbing and electrocatalytic sites or be combined with other electrocatalytic materials and/or semiconductors to form hybrid systems. Pure plasmon metal-driven electrocatalysis combined with effective charge sepa-

[*] S. Ganguli,[+] Z. Zhao,[+] Y. Hattori, J. Sá, A. Sekretareva
Department of Chemistry—Ångström, Uppsala University
75120 Uppsala (Sweden)
E-mail: alina.sekretareva@kemi.uu.se
O. Parlak
Department of Medicine Solna, Center for Molecular Medicine, Karolinska Institute
17176 Stockholm (Sweden)
O. Parlak
Center for the Advancement of Integrated Medical and Engineering Science, Karolinska Institutet and KTH Royal Institute of Technology
17177 Stockholm (Sweden)
J. Sá
Institute of Physical Chemistry, Polish Academy of Sciences
01224 Warsaw (Poland)
[+] These authors contributed equally to this work.

[**] A previous version of this manuscript has been deposited on a preprint server (https://doi.org/10.26434/chemrxiv-2023-wbztb).

ration strategies is proposed to be more efficient than electrocatalysis on metal/semiconductor interfaces, as the Schottky barrier limits the collection efficiency of hot carriers.[19] In the Schottky-junction-free systems, the plasmonic nanostructures on a conductive support or themselves act as a working electrode that drives the electrocatalytic reaction. A suitable potential bias is applied to this electrode to extract either hot electrons in the case of oxidation reactions or holes for reduction reactions to the external circuit. It is suggested that in this way, the potential bias prevents charge recombination and leads to the accumulation of specific hot charge carriers, the injection of which accelerates the electrocatalytic reaction.[2] Enhancement of several electrocatalytic reactions in the direct Schottky-junction-free systems due to participation of hot carriers has been reported.[8,14,20,21]

Understanding the intrinsic mechanism of PEEC using conventional ensemble measurements is challenging due to averaging of the recorded catalytic currents over the heterogeneous distribution of many plasmonic nanostructures and active sites. To separate the contributions of various LSPR effects to the mechanism of rate enhancement in PEEC, well-defined confined geometries are required, which are easier to achieve using single-particle methods.[22] However, most PEEC studies have been done using macroelectrodes with randomly immobilized plasmonic particles. There are only a few reports where PEEC on single nanoparticles was investigated.[23,24] For example, Willets group used scanning electrochemical microscopy (SECM) to monitor hot carrier generation on single gold nanoparticles (AuNPs) attached to an indium tin oxide electrode directly or with an intermediate layer of semiconducting TiO_2.[25,26] They were able to quantify the relative contribution of thermal effects and hot carriers in plasmon-enhanced electrooxidation[25] and assess the thermalized hot carrier energy distribution after the electron injection to the semiconductor layer.[26] Zhou et al. applied single-entity electrochemistry (SEE) of collision (also called nano-impact SEE) to investigate proton electroreduction on a cobalt metal-organic framework (Co-MOF) nanosheet layer deposited on a carbon ultramicroelectrode. The Co-MOF acts as an intermediate layer between the carbon ultramicroelectrode and plasmonic Ag/Au nanoparticles. Upon collision of single Ag/Au nanoparticles under irradiation, increased catalytic currents were observed that have been attributed to hot carrier injection from the nanoparticle to Co-MOF, leading to lowering of the reaction activation energy.[27]

Here, we use nano-impact SEE to investigate glucose electrooxidation on AuNPs at the single-particle level in a pure plasmon metal system. We first measure hot carrier dynamics in AuNPs under experimental conditions using transient absorption spectroscopy (TAS). We then compare the intrinsic photoelectrocatalytic activity of single AuNPs to photocurrents recorded in ensemble measurements on nanoparticles attached to conductive supports. Our results demonstrate how immobilizing AuNPs on a potentially biased conductive support can alter the cause of current enhancement in PEEC, suppressing the contribution of plasmonic effects. This holds true when switching the electrocatalytic reaction from oxidation to reduction, as demonstrated by oxygen reduction on AuNPs. This work highlights the limitation of widely used conventional ensemble electrochemical setups in PEEC measurements in pure plasmon metal systems and puts forward the nano-impact electrochemistry method as a promising alternative.

Results and Discussion

This study used reactant-free AuNPs with an average size of 18 ± 4 nm as measured by transmission electron microscopy (TEM) (Figure 1A) as a plasmonic electrocatalytic material. AuNPs in 10 mM NaOH, 50 mM glucose solution (experimental conditions in SEE for glucose oxidation on AuNPs) show an absorption maximum at 515 nm, which is slightly shifted from that of the as-received stabilized solution of AuNPs at 518 nm. (Figure 1B). The absorption maximum is consistent with the LSPR band of free electrons in spherical AuNPs.[28]

To explore hot carrier dynamics in the AuNPs/glucose system, we performed transient absorption spectroscopy (TAS) measurements. The excitation wavelength (pump) was set to $\lambda = 550$ nm, close to the LSPR peak of AuNPs and the laser wavelength used further in the electrocatalytic studies. As the excitation pump is set to a higher wavelength relative to the LSPR peak, it eliminates any contribution from Au interband transitions.[29,30] Figure 1C shows the temporal evolution of the difference in absorption ($\Delta Abs = Abs_{pump} - Abs_{unpump}$), where the ΔAbs is ascribed to free pump-laser-induced heating of the electron distribution,[31,32] i.e., generation of hot carriers. The excitation of the plasmon broadens the plasmon absorption peak. The pump-probe results in a signal consisting of bleach around the central absorption peak and two winglets on each side. Figure 1D shows temporal changes of the ΔAbs at the peak of the LSPR bleach (518 nm) in 10 mM NaOH solution with and without glucose. Both traces can be fitted by a biexponential decay function with the decay constants of 3.54 ± 0.07 ps for the solution without glucose and 3.71 ± 0.07 ps for the solution with glucose for the fast decaying component and 293 ± 5 ps for both solutions for the slow decaying component. The faster decaying component is assigned to the thermal equilibration process between the electron and lattice systems (electron-phonon scattering), while the longer decaying component relates to phonon-phonon scattering.[32] Comparison of the ΔAbs traces in the presence and absence of glucose in the solution indicates that glucose does not alter the hot carrier generation and decay processes and does not shift LSPR peak.

The electrocatalytic activity of AuNPs towards glucose oxidation was first examined by conventional ensemble electrochemistry in a three-electrode setup.[18] A highly oriented pyrolytic graphite electrode (HOPG) with immobilized AuNPs (AuNP/HOPG) was used as a working electrode. HOPG was chosen as an electrode support because of its similar properties with a carbon microfibre, which was used as the working electrode for SEE measurements (see below). Figure 2A displays representative linear

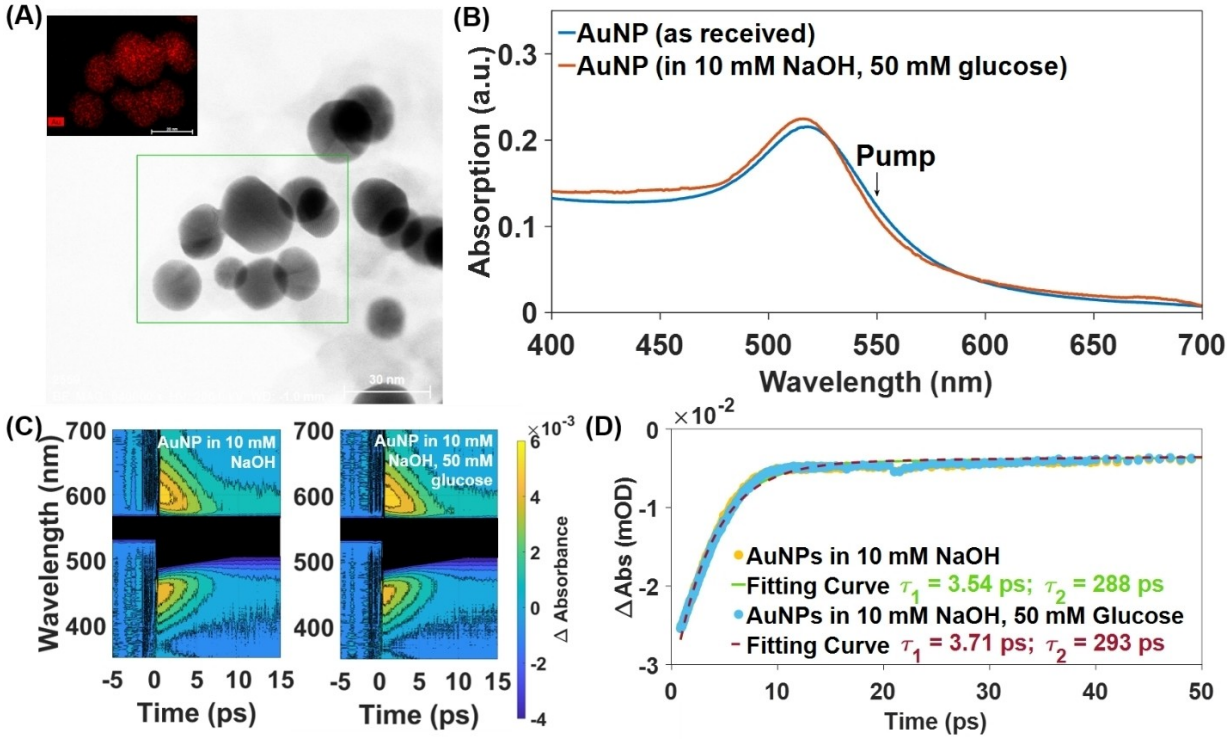

Figure 1. A) STEM image and EDS mapping (inset) of the AuNPs. B) UV/Vis electronic absorbance spectra of the as-received stabilized solution of AuNPs (blue) and solution of AuNPs in 10 mM NaOH, 50 mM glucose (orange). C) Two-dimensional color maps of the temporal evolution of the surface plasmon resonance of AuNPs in 10 mM NaOH, and in 10 mM NaOH, 50 mM glucose. The black box denotes the spectral region obscured by the pump pulse. D) Kinetic trace extracted at 518 nm, corresponding to the bleach of the plasmon peak due to surface-plasmon optical excitation.

sweep voltammograms (LSVs) recorded on the AuNP/HOPG electrodes in a deoxygenated aqueous solution of 100 mM NaOH and 30 mM glucose in the dark (black curve) and under irradiation with a 532 nm laser (green curve). Two well-defined peaks are observed at ≈ −0.4 and 0.2 V vs. Ag/AgCl on the LSVs, which are not present on bare HOPG electrodes in the absence of AuNPs (Figure S1). Based on a combination of electrochemical measurements, surface-enhanced resonance Raman (SERS) and DFT calculations, it has been previously shown that glucose electrooxidation starts at a potential region, where the gold surface is not yet fully oxidized and is dominated by the dehydrogenating adsorption of glucose followed by its oxidation into gluconate.[33,34] Thus, the first peak can be ascribed to the electrooxidation of electrochemically adsorbed glucose molecules into gluconate, and the latter represents a competitive or parallel oxidation of glucose and gluconate into glucaric acid.[35,36]

Upon illumination of the electrode by the 532 nm laser, an increase of the Faradaic anodic current by 39 ± 7 % for the current peak at 0.2 V vs. Ag/AgCl is evident. The photocurrent (the difference between the catalytic current in the dark and under illumination) was previously attributed to the hot-hole-assisted electrooxidation of glucose, where the fast decay of hot carriers (of $\approx 2.7 \times 10^{11}$ s^{-1} based on our TAS measurements) is inhibited by the suitable potential bias driving hot electrons into the external circuit.[8,9] Chronoamperometry measurements under alternating illumination can be used to distinguish hot carriers and temperature contributions in PEEC when the response time of the cell is known, and it is fast.[18,37] Figure 2B shows the photocurrent response of the AuNP/HOPG electrode under alternating illumination in the deoxygenated 100 mM NaOH and 30 mM glucose solution. The relative anodic current enhancement in chronoamperometry differs from the values obtained from the LSV peak current as both glucose and gluconate can be oxidized at the applied potential. Their relative concentrations on the experimental timescale differ depending on the employed experimental technique.[36]

However, the rise and fall of the photocurrent correspond to the turning on (green areas in Figure 2B) and off (grey areas in Figure 2B) of the light source. The decay of the photocurrent after turning off the illumination is gradual and much slower than the cell time constant ($\tau_{RC} = 30$ ms; Figure S2, Note S1) and the lifetime of hot carriers quantified by the TAS measurements, implying that the contribution of hot carriers to glucose electrocatalysis is minimal and that thermal effects are the primary source of electrooxidation rate enhancement.[18] LSVs on AuNP/HOPG electrodes illuminated by a 650 nm laser at which hot carriers can not be generated also show an increase of the peak current at 0.2 V by 37 ± 6 % (Figure 2C). This matches within the error to the increase observed under 532 nm illumination (Figure 2C vs. Figure 2A).[38] Similarly, the

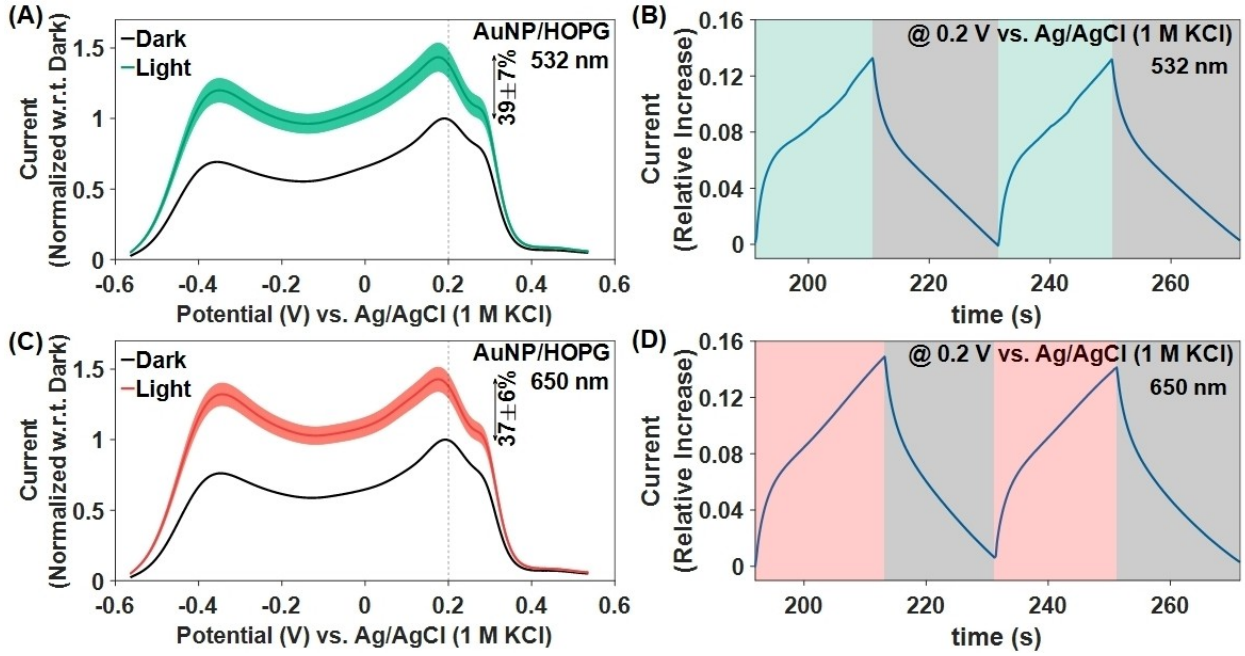

Figure 2. A), C) LSV scans on AuNP/HOPG electrodes in the dark (black trace) and under illumination A) with 532 nm laser (green trace), and C) with 650 nm laser (red trace) of the same intensities (see Experimental Section). The current under illumination is normalized to the peak current of respective dark values. The voltammograms were recorded thrice to compute the mean values and the standard deviations. The standard deviations for currents recorded under illumination at different applied potentials are shown as shaded regions. B), D) Chronoamperometry measurements on AuNP/HOPG under alternating illumination at a fixed applied potential of 0.2 V vs. Ag/AgCl (1 M KCl). Illumination source: B) 532 nm laser and D) 650 nm laser of the same intensities. All measurements were performed in the deoxygenated 30 mM glucose, 100 mM NaOH solution.

photocurrent response in chronoamperometry under 650 nm illumination is almost identical to the photocurrent under 532 nm illumination (Figure 2D vs. Figure 2B). These data demonstrate that the observed enhancement of electrocatalytic glucose oxidation on AuNP/HOPG electrodes is not due to AuNP LSPR. The controlled experiment performed with an ITO working electrode modified with AuNPs (AuNP/ITO) showed an increase of the photocurrent by only 4 % and 1.7 % at 532 nm and 650 nm, respectively (Figure S3). Comparison between the absorption spectra of AuNP/HOPG and AuNP/ITO electrodes reveals that the absorption of AuNP/HOPG is significantly higher compared to AuNP/ITO, and the absorption spectrum of the AuNP/HOPG electrode is dominated by HOPG rather than AuNPs absorption (Figure S4, Note S2). These differences in electrocatalytic performance and absorption spectra between AuNP/HOPG and AuNP/ITO indicate that photo-induced heating of HOPG rather than the decay of plasmons is the primary source of the electrocatalytic rate enhancement on AuNP/HOPG electrodes, in agreement with our previous findings.[18]

Heterogeneities in nanoparticle size, shape, and interaction with the support contribute to the observed electrocatalytic properties of plasmonic photoelectrodes in PEEC.[39] To accurately measure intrinsic nanoparticle reactivity and minimize collective heating effects,[40] we further studied PEEC of glucose electrooxidation on individual AuNPs using nano-impact SEE. In nano-impact SEE experiments, individual AuNPs freely diffusing in solution time to time approach and collide with the surface of a potentially-biased ultramicroelectrode (UME), provoking glucose electrooxidation on the surface of the NP. This causes current spikes on the *i–t* curve, with each spike corresponding to electrocatalytic glucose oxidation on an individual AuNP impacting the electrode (Scheme 1).

Prior SEE experiments, the stability of AuNPs suspension in alkaline glucose solution was investigated by dynamic light scattering (DLS) and zeta potential measurements (Figures S5, S6, Note S3), which showed that AuNPs agglomeration was negligible on the timescale of measurements only in 10 mM NaOH solution. At the same time, higher concentrations of NaOH resulted in fast agglomeration of nanoparticles. The SEE measurements were therefore performed in 10 mM NaOH solution. A carbon fiber UME (CF-UME) was inserted as the working electrode in a deoxygenated 10 mM NaOH, 50 mM glucose aqueous solution containing 5 pM of AuNPs. As the AuNP surface oxidizes and loses its electrocatalytic activity at high potentials (Figure S7, Note S4), 0.2 V vs. Ag/AgCl, corresponding to the peak potential in the LSV curves (Figure 2A, C), was chosen for chronoamperometry measurements (measurements at lower potentials, i.e. 0.1 V vs. Ag/AgCl generated current signals that were on the level of the background noise, Figure S8). Figure 3 shows representative signals registered in the dark (Figure 3A, D), and under illumination with 532 nm (Figure 3B, E) and 650 nm lasers

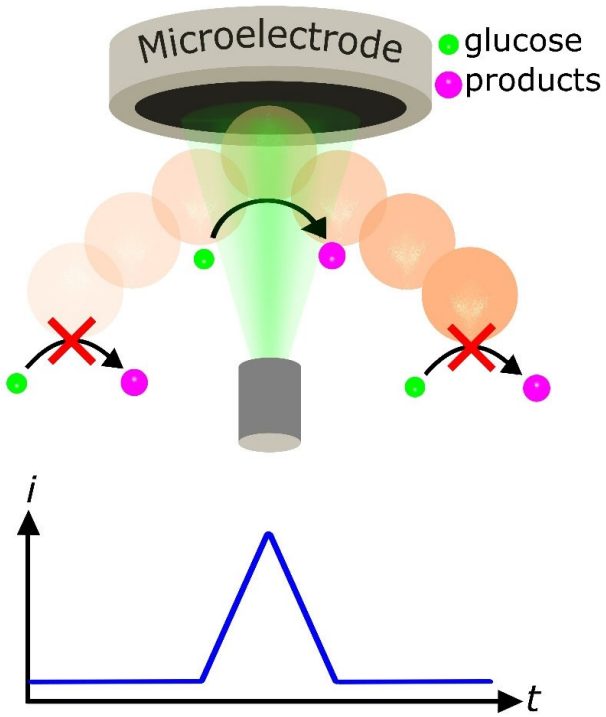

Scheme 1. Schematic illustration of the nano-impact SEE experiment with plasmonic nanoparticles under illumination.

(Figure 3C, F). Oxidative current transients were observed in all cases.

To verify that the spikes originate from the electrooxidation of glucose on AuNPs in contact with the CF-UME, we performed several control experiments. No current spikes were observed in NaOH/glucose solution without AuNPs (Figure S9A). It has been suggested earlier that OH^- acts as a hole scavenger in plasmon-driven catalysis, which then, in the form of $^{\bullet}OH$ radicals, diffuses through the solution to oxidize glucose.[8] However, we did not observe any current transients when only OH^- and AuNPs were present in the solution (Figure S9B). Thus, both AuNPs and glucose are required to observe catalytic currents in the dark (in agreement with earlier reported collision electrochemistry of AuNPs[41]) and under illumination. The collision frequency scales linearly with the particle concentration (Figure S10), indicating that detected signals correspond to nano-impacts of single particles.

The detection of oxidative spikes and quantification of associated charges were conducted using an in-house developed data analysis algorithm (details in Experimental Section). Figure 4A–C show histograms of the charge corresponding to each nanoparticle collision in the dark (Figure 4A), and under illumination with 532 nm (Figure 4B) and 650 nm lasers (Figure 4C). The mean charge for collisions in the dark was found to be 0.870 ± 0.034 fC, for collisions under 532 nm laser illumination, 1.230 ± 0.058 fC, and for collisions under 650 nm, 0.920 ± 0.036 fC (the standard error of the mean is calculated as $\sigma/\sqrt{n}$, where σ is the standard deviation of the normal distribution, n is the sample size). As was assessed via the Mann-Whitney U test (Note S5), the difference between the data collected in the dark and under 532 nm laser illumination is statistically significant. In comparison, there is no significant difference between the dark data and data under 650 nm illumination. Figure 4D displays histograms of the average duration of the spikes in the dark and under illumination with 532 nm and 650 nm lasers. Under 532 nm laser irradiation, a portion of current spikes lasted longer than 350 ms, which was not observed in the dark or under 650 nm laser irradiation.

Contrary to the bulk measurements (Figure 2A, C), different rate enhancements were detected at different wavelengths, with the charge per spike being higher for measurements under 532 nm illumination. The absorption spectrum of carbon fibers used as the working electrode in SEE measurements (Figure S11) is similar to that of HOPG electrodes (Figure S4), with no significant difference in absorption at 650 and 532 nm. Therefore, the observed wavelength dependence of the photocurrent suggests that AuNPs LSPR leads to electrocatalytic rate enhancement in SEE, unlike in ensemble measurements on HOPG electrodes. Both highly energetic charge carriers and the local temperature increase caused by their thermalization can contribute to the observed rate enhancement under 532 nm laser illumination.

For PEEC in ensemble measurements, it has been shown earlier that plasmon-induced heating can lead to higher photocurrents due to the increased mass transport rate of a substrate to the electrode surface.[25] For the SEE measurements, the magnitude of the current spikes can be compared to values expected for a diffusion-limited reaction on a spherical nanoparticle in contact with a planar electrode according to:[42]

$$I = 4\pi(ln2)nFDCr \tag{1}$$

where D is the diffusion coefficient of reactants (glucose) at concertation of C, F is the Faraday's constant, and r is the radius of the NP. For our system, the values are $n=2$, $D=6.7\times10^{-6}\ cm^2\,s^{-1}$,[43] and $r=10$ nm, giving the limiting current of $\approx$560 pA. The detected current transients in the dark and under illumination are significantly smaller, showing that the reaction is not mass transfer-controlled. Thus, the contribution of increased mass transport due to local heating to the observed photocurrents can be excluded.

We have previously shown that increased temperature under illumination can facilitate charge transfer kinetics.[18] Temperature increase contribution to the interfacial electron transfer rate (k) at a fixed applied potential can be estimated using the Arrhenius equation:

$$\frac{k(T_1)}{k(T_2)} = exp\left[-\frac{E_A}{R}\left(\frac{1}{T_1}-\frac{1}{T_2}\right)\right] \tag{2}$$

where T_1 and T_2 are two different temperatures, E_A is the activation energy of the reaction, R is the gas constant.

To obtain E_A of glucose electrooxidation on gold, we performed LSVs under kinetic control conditions in the dark in the deoxygenated 100 mM NaOH and 30 mM glucose solution at different temperatures, which were

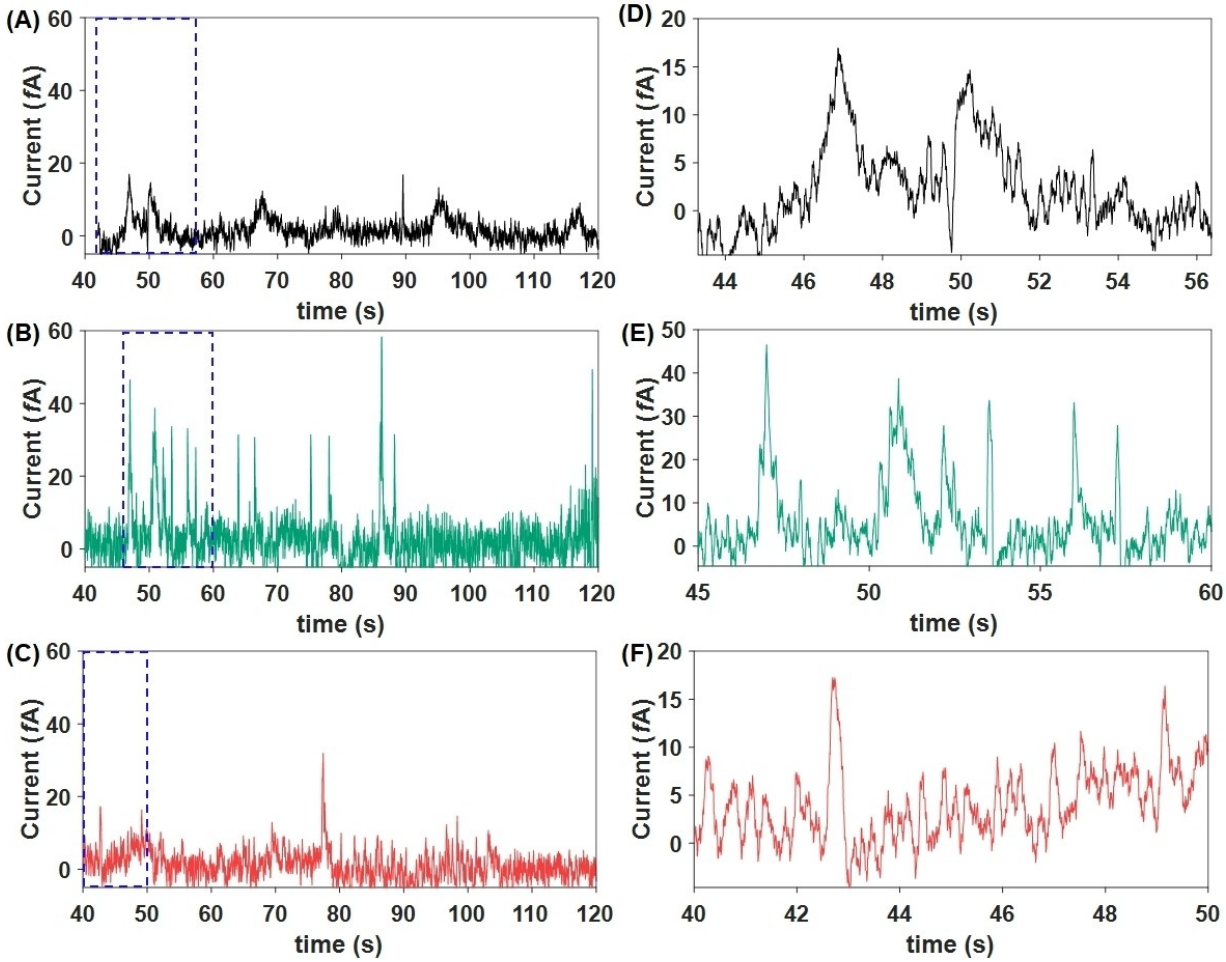

Figure 3. Representative *i–t* curves recorded on a CF-UME in the deoxygenated 10 mM NaOH, 50 mM glucose aqueous solution upon collisions of 5 pM AuNPs A), D) in the dark, and under illumination with (B), E) 532 nm laser and (C), F) 650 nm laser of the same intensities. D), E), and F) are zoomed areas (denoted by the blue box) of A), B), and C), respectively. The CF-UME was biased at 0.01 V vs. ground, which corresponds to 0.2 V vs. Ag/AgCl (1 M KCl).

varied externally using a thermostat. Measurements were taken with a rotating disk electrode setup at various rotation rates to ensure kinetic control of the current. At rotation rates of 1000 rpm and higher, the peak current at 0.2 V vs. Ag/AgCl was independent of the rotation rate (Figure S12), as expected for a kinetically controlled reaction (the peak is observed instead of the steady-state plateau current expected under kinetic control conditions due to the inactivation of the gold surface at higher applied potentials as discussed previously[18]). Figure 5A shows representative LSVs recorded on a gold RDE at a 2500 rpm rotation rate with temperatures of the solution varied from 18.6 °C to 30.8 °C. Peak currents at 0.2 V vs Ag/AgCl increase with increasing solution temperature and their values were used to calculate the activation energy of glucose electrooxidation at this potential (Figure 5B). E_A was found to be 32.9 kJ mol^{-1}.

Charge/nano-impact in SEE under kinetic control conditions is directly proportional to the rate of glucose electrocatalysis on an individual AuNP. Assuming that the increase of the current signal under 532 nm illumination is entirely due to the thermal facilitation of the charge transfer kinetics, a temperature increase can be estimated from Equation (2) using E_A for glucose electrooxidation on gold at 0.2 V vs. Ag/AgCl. An average temperature increase of ≈8 °C will lead to a charge/nano-impact increase consistent with the recorded experimental data (Figure 5A, B). We would like to point out that as catalysis occurs at the nanoparticle surface, the calculated value reflects the effective average temperature of the surface and not the temperature of the hot spots or the bulk of the material.[44]

We have performed photocurrent measurements of glucose electrooxidation on AuNPs under illumination with a conventional ensemble electrochemistry setup (Figure 2) and at the single-particle level using nano-impact SEE (Figure 3). Two irradiation wavelengths, one corresponding to LSPR of AuNPs where generation of hot carriers occurs (532 nm) and one that can not account for any hot charge carrier effects (650 nm), were chosen to distinguish photothermal from LSPR contribution to electrocatalysis.[38] The photocurrent response in ensemble measurements was independent of the wavelength. In contrast, a significant

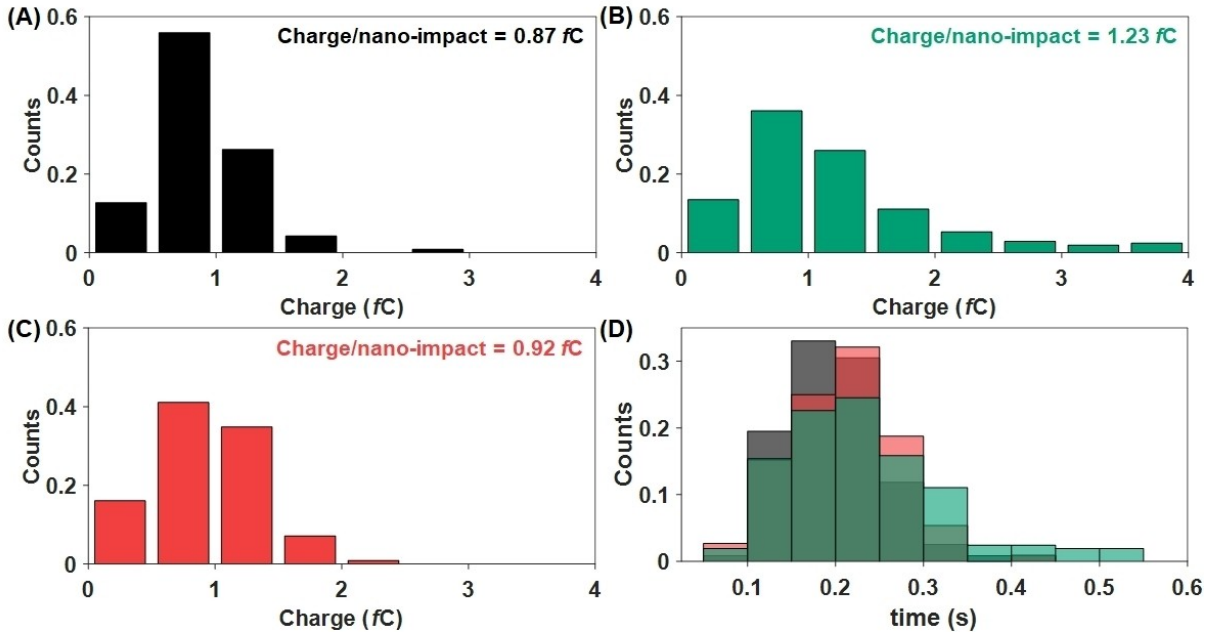

Figure 4. The charge histograms, bin size 0.5 fC for SEE data collected A) in the dark, and under illumination with the B) 532 nm laser and C) 650 nm laser of the same intensities. D) The histogram of duration of nano-impacts, bin size 0.05 s, for single collisions in the dark (grey), and under 532 nm laser (green) and 650 nm laser (red) illuminations. All data were recorded with a CF-UME biased at 0.01 V vs. ground, corresponding to 0.2 V vs. Ag/AgCl (1 M KCl) in the deoxygenated 10 mM NaOH, 50 mM glucose aqueous solution containing 5 pM AuNPs.

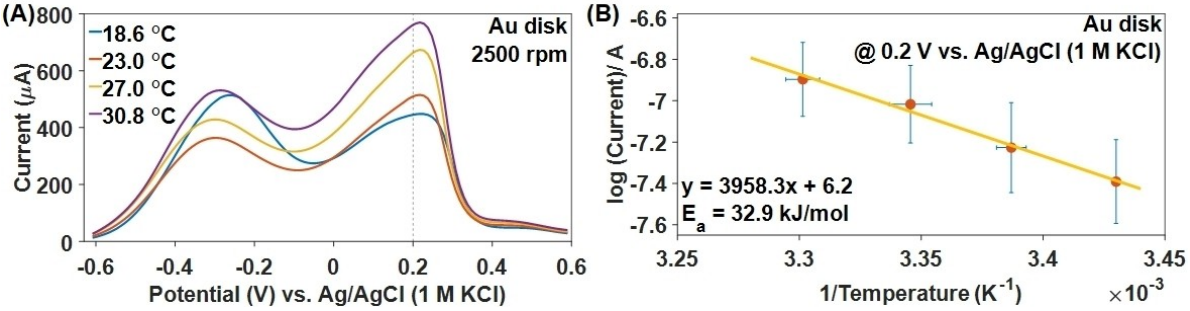

Figure 5. A) LSV scans on the gold disk electrode in the deoxygenated 30 mM glucose, 100 mM NaOH solution in the dark at different temperatures varied externally. B) Determination of the activation energy for glucose electrooxidation at 0.2 V vs. Ag/AgCl (1 M KCl). The voltammograms were recorded thrice to compute the population mean value and the corresponding standard deviation.

dependence of the response on the illumination wavelength was observed in SEE measurements (Table 1). This effect was preserved when we switched the electrocatalytic reaction from oxidation to reduction using oxygen reduction on AuNPs as a model system (Figure S13, Note S6).

Table 1: Relative enhancements of glucose electrooxidation currents in PEEC on AuNPs and different electrodes under irradiations with 532 nm and 650 nm lasers, and the primary absorber in each case.

Electrode	532 nm	650 nm	Absorber
AuNP/HOPG	39 ± 7%	37 ± 6%	HOPG
AuNP/ITO	4%	1.7%	AuNP
CUME	41%	5%	AuNP

In ensemble measurements on HOPG electrodes with immobilized AuNPs, the wavelength independence of the electrocatalytic photocurrents at 532 nm and 650 nm corresponding to approximately identical absorbance of the electrode (Figure S4) suggests a minimal contribution of LSPR to electrocatalysis. Temperature effects due to HOPG absorption dominate the observed photocurrent. This is further confirmed by control experiments on AuNP/ITO electrodes (Figure S3), where only a minor current increase of ≈4% was detected under 532 nm illumination and 1.7% under 650 nm illumination for glucose electrooxidation. Thus, electrocatalysis enhancement by plasmonic effects is minimal for AuNPs immobilized on conductive support in accordance with our earlier results.[18]

When AuNPs are in direct contact with the electrode support (HOPG or ITO) connected to an external voltage

source, the Fermi level (E_F) of the AuNPs is equilibrated with the E_F of the electrode, which is defined by the applied potential.[45] For the system under external potential control, upon continuous illumination, the energy of the generated hot electrons is always higher, and the energy of the hot holes is always lower than the E_F of the working electrode. Thus, the generated hot carriers perturb the potential of the electrode, and this perturbation will be eliminated by filling up hot holes by electron transfer from the electrode to AuNPs, at the same time hot electrons with energies higher than E_F of the electrode will be removed to the external circuit. Electron transfer between the electrode and the AuNPs is usually faster than the redox reaction at the particle surface.[45] As a result, the hot carriers generated in AuNPs in direct contact with the working electrode will be quenched before being able to participate in a chemical reaction, e.g. glucose oxidation or oxygen reduction. This will also minimize any heating of the lattice originating from hot charge carrier recombination. Therefore, we propose that the fast equilibration of the Fermi levels is the cause of the lack of significant contribution of plasmonic effects in ensemble PEEC when plasmonic nanomaterials are directly immobilized on conductive electrode supports or themselves act as a working electrode.

In nano-impact SEE experiments, a current signal is observed when an AuNP is either in contact with the electrode or within a short distance (<1.5 nm)[46] from the electrode surface that enables charge transfer by tunneling through the electrolyte layer. Far from the electrode surface, the E_F of the AuNP, and therefore the energy of hot carriers, is not affected by the working electrode potential. But even within the charge transfer distance from the electrode, equilibration of E_F levels between the electrode and the AuNP does not necessarily occur in collision experiments when the colliding particle does not stick to the electrode.[45] This is the principal difference between ensemble electrochemistry and SEE measurements for observation of plasmonic effects in PEEC.

The E_F of AuNPs depends on their size, shape, and environment.[46] To roughly estimate the E_F of Au under the experimental conditions, we first measured the open circuit potential (OCP) of an Au-UME in a 10 mM NaOH electrolyte (Figure S14). The addition of glucose shifted the OCP to a lower potential of -0.23 V vs. Ag/AgCl. This is ≈ 0.43 V lower than the potential (0.2 V vs. Ag/AgCl) applied during chronoamperometry measurements.

Considering this estimated difference in E_F between the working electrode (CF-UME) and AuNPs, two possible explanations are proposed for the wavelength-dependent photocurrent enhancement in SEE for glucose electrooxidation (the case of oxygen reduction is analogous with holes replaced by electrons and vice versa). The first possibility is current enhancement due to the injection of hot carriers. When the AuNP is not in direct contact with the electrode to enable rapid E_F equilibration but at a distance sufficient for charge transfer, the hot electrons will be transferred to the working electrode due to significant driving force provided by the large difference in the energies of the electrode and hot electrons (Scheme 2A). At the same time, the hot holes inside the AuNPs can not be neutralized by electron transfer from the electrode at the same rate as hot electrons are removed to the external circuit. This is because the energies of the holes are either higher than that of the electrons at the electrode or only slightly lower depending on the exact value of E_F of the AuNP and the energy distribution of the hot holes.[26] These remaining hot holes participate in charge transfer with glucose molecules. The injection of hot electrons to the electrode is reflected in significantly higher charge (extra $\approx 2\times10^3$ electrons for glucose oxidation and $\approx 2.9\times10^6$ holes for oxygen reduction) transferred per collision under illumination with the 532 nm laser (Figure 4B and Figure S13C) compared to the dark measurements (Figure 4A and Figure S13B) and measurements under 650 nm laser illumination (Figure 4C and Figure S13D). It is important to note that hole transfer to glucose from the AuNP is thermodynamically favorable in the presence of an electron acceptor even without a potential bias. Indeed, glucose catalysis on AuNPs in a solution containing dioxygen as an electron acceptor has been observed.[47] In our experimental setup, this reaction is suppressed since glucose oxidation experiments are performed in deoxygenated solutions. As the hot carrier generation in AuNPs is a wavelength-dependent phenomenon (Figure 1B–D), the participation of hot charge carriers in the catalytic reaction is possible only under 532 nm but not under 650 nm irradiation. Upon contact with the electrode, the Fermi levels of the AuNP and the working electrode will equilibrate, and injection of hot carriers will cease. As the participation of hot carriers is limited to the approach phase, i.e. beginning at the time when charge transfer through tunneling becomes possible and ending after the Fermi levels equilibration, an increase in the duration of the peaks is expected. This has indeed been observed for 532 nm irradiation compared to the dark and 650 nm irradiation (Figure 4D).

The second possibility is the facilitation of the catalytic reaction by thermal contribution due to the recombination of charge carriers. As the suspended AuNPs are exposed to laser irradiation, the hot carriers will recombine leading to lattice heating. When a 532 nm laser-irradiated AuNP comes into contact with the working electrode, thereby becoming active for the catalytic reaction, its temperature can be already higher compared to the AuNP in the dark. The interfacial charge transfer will become faster on the heated AuNP leading to enhanced charge /nano-impact. The increase in the effective average temperature at the nanoparticle surface of $\approx 8\,^{\circ}C$ estimated using Equation (2) for glucose electrooxidation will enhance interfacial charge transfer kinetics consistent with the observed increase in charge/nano-impact under 532 nm illumination (Figure 4A vs. B). In this case, one would not expect a detectable increase in peak duration because there is no significant increase in the driving force (as in the case of hot electrons) sufficient to drive charge transfer at longer distances from the electrode surface.

Above, we considered two extreme cases in which the observed rate enhancement was either entirely attributed to the injection of hot charge carriers or the increase in local

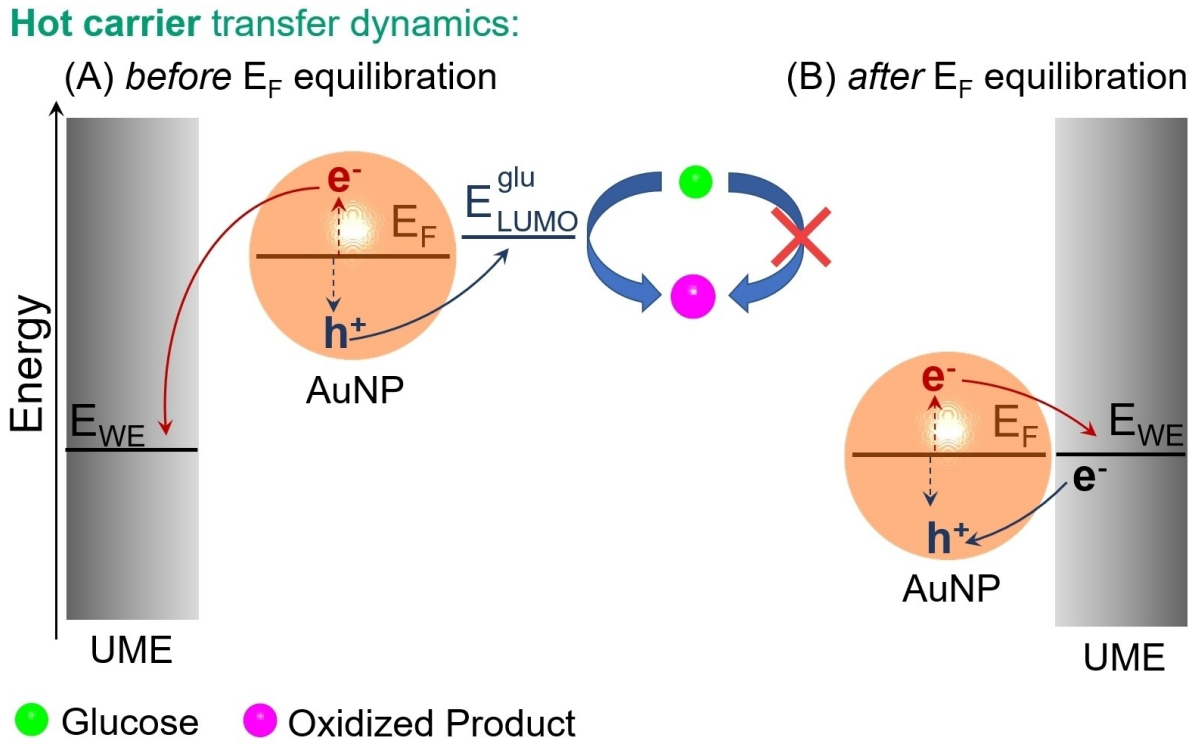

Scheme 2. Under 532 nm illumination, A) within distance allowing charge tunneling and before E_F equilibration, selective transfer of hot electrons from AuNP to the biased electrode promotes hot hole transfer to glucose resulting in glucose oxidation. B) Upon collision and after E_F equilibration, fast quenching of hot carriers (both electrons and holes) by electrode inhibits hot hole-assisted oxidation of glucose.

temperature. In the case of plasmon-enhanced electrocatalysis, which necessarily includes electron transfer, it is challenging to distinguish between the exact contribution of non-thermal hot electrons and thermal electrons whose temperature exceeds the local lattice temperature. The observed increase in peak duration under 532 nm illumination for a fraction of the peaks (Figure 4D) suggests that at least some of the extra charge carriers transferred to the electrode should be highly energetic. Furthermore, it is certain that SEE measurements enable the detection of plasmonic effects in electrocatalysis and the investigation of the intrinsic activity of the plasmonic catalyst at the single-particle level.

Conclusion

We have shown that the contribution of plasmonic effects to electrocatalysis in conventional ensemble electrochemical systems is negligible when direct contact exists between the plasmonic material and the working electrode support.. We propose that this is due to the continuous equilibration of E_F of AuNPs and the working electrode that leads to the neutralization of hot carriers by the voltage source before they can participate in the electrocatalytic reaction. In contrast, nano-impact single-entity electrochemistry enables observation of plasmonic effects in the electrocatalytic system due to the decoupling of Fermi levels of AuNPs and the working electrode. Moreover, the method allows for the quantification of extra charges for electrocatalysis on a single plasmonic nanoparticle due to LSPR. Overall, this study demonstrates the limitations of commonly used conventional ensemble electrochemical setups in PEEC measurements with pure plasmonic metal systems and proposes the nano-impact SEE method as a promising alternative.

Supporting Information

Electrocatalytic glucose oxidation with HOPG and AuNP/HOPG, Cell constant, LSV on AuNP/ITO under dark and illumination, Absorption spectra of AuNP/HOPG, AuNP/ITO, and carbon microfiber, Nanoparticle characterization DLS and Zeta potential, CV of Au disk and AuNP/HOPG, SEE at 0.1 V vs. Ag/AgCl (1 M KCl), controlled collision electrochemistry experiments, Rotating disk measurements, Oxygen reduction reaction; bulk response on AuNP/HOPG vs. in SEE under dark and illumination, OCP determination with Au UME, Supporting Notes.

Acknowledgements

A.S. thanks FORMAS (N 2019-01126) and Göran Gustafsson Stiftelse (nr. 2215) for supporting this research. S.G. acknowledge support from Carl Tryggers Stiftelse (N CTS

19:326). The authors greatly acknowledge Robert Bericat Vadell for his help with the TAS measurements.

Conflict of Interest

The authors declare no competing financial interests.

Data Availability Statement

The data that support the findings of this study are available from the corresponding author upon reasonable request.

Keywords: Collision Electrochemistry · Glucose Oxidation · Hot Charge Carrier · Nano-Impacts · Photoelectrochemistry · Plasmonic Catalysis

[1] E. R. Corson, E. B. Creel, R. Kostecki, B. D. McCloskey, J. J. Urban, *iScience* **2020**, *23*, 100911.
[2] J. Zhao, S. Xue, R. Ji, B. Li, J. Li, *Chem. Soc. Rev.* **2021**, *50*, 12070–12097.
[3] Y. Zhang, S. He, W. Guo, Y. Hu, J. Huang, J. R. Mulcahy, W. D. Wei, *Chem. Rev.* **2018**, *118*, 2927–2954.
[4] K. Awazu, M. Fujimaki, C. Rockstuhl, J. Tominaga, H. Murakami, Y. Ohki, N. Yoshida, T. Watanabe, *J. Am. Chem. Soc.* **2008**, *130*, 1676–1680.
[5] Z. Liu, W. Hou, P. Pavaskar, M. Aykol, S. B. Cronin, *Nano Lett.* **2011**, *11*, 1111–1116.
[6] X. Li, D. Xiao, Z. Zhang, *New J. Phys.* **2013**, *15*, 023011.
[7] Z. Zhang, C. Zhang, H. Zheng, H. Xu, *Acc. Chem. Res.* **2019**, *52*, 2506–2515.
[8] C. Wang, X.-G. Nie, Y. Shi, Y. Zhou, J.-J. Xu, X.-H. Xia, H.-Y. Chen, *ACS Nano* **2017**, *11*, 5897–5905.
[9] M. Rodio, M. Graf, F. Schulz, N. S. Mueller, M. Eich, H. Lange, *ACS Catal.* **2020**, *10*, 2345–2353.
[10] L. Huang, J. Zou, J.-Y. Ye, Z.-Y. Zhou, Z. Lin, X. Kang, P. K. Jain, S. Chen, *Angew. Chem. Int. Ed.* **2019**, *58*, 8794–8798; *Angew. Chem.* **2019**, *131*, 8886–8890.
[11] H. Yang, L.-Q. He, Y.-W. Hu, X. Lu, G.-R. Li, B. Liu, B. Ren, Y. Tong, P.-P. Fang, *Angew. Chem. Int. Ed.* **2015**, *54*, 11462–11466; *Angew. Chem.* **2015**, *127*, 11624–11628.
[12] H. Yang, Z.-H. Wang, Y.-Y. Zheng, L.-Q. He, C. Zhan, X. Lu, Z.-Q. Tian, P.-P. Fang, Y. Tong, *J. Am. Chem. Soc.* **2016**, *138*, 16204–16207.
[13] M. Rasmussen, A. Serov, K. Artyushkova, D. Chen, T. C. Rose, P. Atanassov, J. M. Harris, S. D. Minteer, *ChemElectroChem* **2019**, *6*, 241–245.
[14] E. Contreras, R. Nixon, C. Litts, W. Zhang, F. M. Alcorn, P. K. Jain, *J. Am. Chem. Soc.* **2022**, *144*, 10743–10751.
[15] R. Wan, S. Liu, Y. Wang, Y. Yang, Y. Tian, P. K. Jain, X. Kang, *Nano Lett.* **2022**, *22*, 7819–7825.
[16] F. Shi, J. He, B. Zhang, J. Peng, Y. Ma, W. Chen, F. Li, Y. Qin, Y. Liu, W. Shang, P. Tao, C. Song, T. Deng, X. Qian, J. Ye, J. Wu, *Nano Lett.* **2019**, *19*, 1371–1378.
[17] X. Zhang, X. Li, M. E. Reish, D. Zhang, N. Q. Su, Y. Gutiérrez, F. Moreno, W. Yang, H. O. Everitt, J. Liu, *Nano Lett.* **2018**, *18*, 1714–1723.
[18] S. Ganguli, A. Sekretareva, *ACS Catal.* **2022**, *12*, 4110–4118.
[19] Y. Zhang, W. Guo, Y. Zhang, W. D. Wei, *Adv. Mater.* **2021**, *33*, 2006654.
[20] Y. Kim, E. B. Creel, E. R. Corson, B. D. McCloskey, J. J. Urban, R. Kostecki, *Adv. Energy Mater.* **2018**, *8*, 1800363.
[21] M. Graf, G. B. Vonbun-Feldbauer, M. T. M. Koper, *ACS Nano* **2021**, *15*, 3188–3200.
[22] J. J. Baumberg, *Faraday Discuss.* **2019**, *214*, 501–511.
[23] R. F. Hamans, R. Kamarudheen, A. Baldi, *Nanomaterials* **2020**, *10*, 2377.
[24] Z. Liang, J. Li, Y.-G. Zhou, *Chem. Eur. J.* **2022**, *28*, e202201489.
[25] Y. Yu, V. Sundaresan, K. A. Willets, *J. Phys. Chem. C* **2018**, *122*, 5040–5048.
[26] Y. Yu, K. D. Wijesekara, X. Xi, K. A. Willets, *ACS Nano* **2019**, *13*, 3629–3637.
[27] W. Zhang, J. Li, X.-H. Xia, Y.-G. Zhou, *Angew. Chem. Int. Ed.* **2022**, *61*, e202115819.
[28] S. Eustis, M. A. El-Sayed, *Chem. Soc. Rev.* **2006**, *35*, 209–217.
[29] M. Bernardi, J. Mustafa, J. B. Neaton, S. G. Louie, *Nat. Commun.* **2015**, *6*, 7044.
[30] L. van Turnhout, Y. Hattori, J. Meng, K. Zheng, J. Sá, *Nano Lett.* **2020**, *20*, 8220–8228.
[31] J. H. Hodak, I. Martini, G. V. Hartland, *J. Phys. Chem. B* **1998**, *102*, 6958–6967.
[32] H. Inouye, K. Tanaka, I. Tanahashi, K. Hirao, *Phys. Rev. B* **1998**, *57*, 11334–11340.
[33] Y. Holade, H. Guesmi, J.-S. Filhol, Q. Wang, T. Pham, J. Rabah, E. Maisonhaute, V. Bonniol, K. Servat, S. Tingry, D. Cornu, K. B. Kokoh, T. W. Napporn, S. D. Minteer, *ACS Catal.* **2022**, *12*, 12563–12571.
[34] M. Pasta, F. La Mantia, Y. Cui, *Electrochim. Acta* **2010**, *55*, 5561–5568.
[35] G. Moggia, J. Schalck, N. Daems, T. Breugelmans, *Electrochim. Acta* **2021**, *374*, 137852.
[36] N. Schlegel, G. K. H. Wiberg, M. Arenz, *Electrochim. Acta* **2022**, *410*, 140023.
[37] C. Zhan, B.-W. Liu, Y.-F. Huang, S. Hu, B. Ren, M. Moskovits, Z.-Q. Tian, *Nat. Commun.* **2019**, *10*, 2671.
[38] G. Baffou, I. Bordacchini, A. Baldi, R. Quidant, *Light: Sci. Appl.* **2020**, *9*, 108.
[39] S. Goines, J. E. Dick, *J. Electrochem. Soc.* **2020**, *167*, 037505.
[40] H. H. Richardson, Z. N. Hickman, A. O. Govorov, A. C. Thomas, W. Zhang, M. E. Kordesch, *Nano Lett.* **2006**, *6*, 783–788.
[41] Y. Liu, B. J. J. Austen, T. Cornwell, R. D. Tilbury, M. A. Buntine, A. P. O'Mullane, D. W. M. Arrigan, *Electrochem. Commun.* **2017**, *77*, 24–27.
[42] X. Xiao, F.-R. F. Fan, J. Zhou, A. J. Bard, *J. Am. Chem. Soc.* **2008**, *130*, 16669–16677.
[43] L. A. Larew, D. C. Johnson, *J. Electroanal. Chem. Interfacial Electrochem.* **1989**, *262*, 167–182.
[44] Q.-Y. Wang, Y.-Y. Chen, R.-K. Ye, Q. Liu, H.-Y. Chen, H. Yang, M.-Y. Li, J.-Q. Hu, P.-P. Fang, *Anal. Chem.* **2021**, *93*, 15517–15524.
[45] P. Peljo, M. D. Scanlon, A. J. Olaya, L. Rivier, E. Smirnov, H. H. Girault, *J. Phys. Chem. Lett.* **2017**, *8*, 3564–3575.
[46] P. Peljo, J. A. Manzanares, H. H. Girault, *Chem. Sci.* **2017**, *8*, 4795–4803.
[47] N. J. Lang, B. Liu, J. Liu, *J. Colloid Interface Sci.* **2014**, *428*, 78–83.

Manuscript received: February 16, 2023
Accepted manuscript online: April 20, 2023
Version of record online: May 9, 2023